THE JOURNAL OF PHYSICAL CHEMISTRY LETTERS
A JOURNAL OF THE AMERICAN CHEMICAL SOCIETY

pubs.acs.org/JPCL

Letter

Ionic Atmosphere Effect on the Absorption Spectrum of a Flavoprotein: A Reminder to Consider Solution Ions

Benjamin D. Dratch, Yoelvis Orozco-Gonzalez, Giovanni Gadda,* and Samer Gozem*

Cite This: *J. Phys. Chem. Lett.* 2021, 12, 8384−8396

Read Online

ACCESS | Metrics & More | Article Recommendations | Supporting Information

ABSTRACT: This study utilizes the FMN-dependent NADH:quinone oxidoreductase from *Pseudomonas aeruginosa* PAO1 to investigate the effect of introducing an active site negative charge on the flavin absorption spectrum both in the absence and presence of a long-range electrostatic potential coming from solution ions. There were no observed changes in the flavin UV−visible spectrum when an active site tyrosine (Y277) becomes deprotonated *in vitro*. These results could only be reproduced computationally using average solvent electrostatic configuration (ASEC) QM/MM simulations that include both positive and negative solution ions. The same calculations performed with minimal ions to neutralize the total protein charge predicted that deprotonating Y277 would significantly alter the flavin absorption spectrum. Analyzing the distribution of solution ions indicated that the ions reorganize around the protein surface upon Y277 deprotonation to cancel the effect of the tyrosinate on the flavin absorption spectrum. Additional biochemical experiments were performed to test this hypothesis.

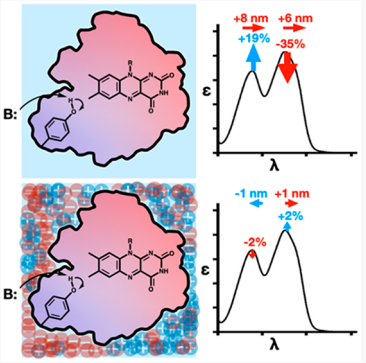

Ions are well-known to modulate the function of lipids, nucleic acids, and proteins.[1−5] For instance, ionizable residues in the active sites of enzymes can promote substrate binding or catalysis,[6−8] while charged residues on protein surfaces stabilize protein structure and protein−protein interactions in biological media.[9,10] Monoatomic solution ions also play an important role in the structural stability and solubility of proteins and nucleic acids.[11−15] However, the delicate interplay between monatomic solution ions, buried charges, and surface charges and their roles in modulating structural stability is not as well understood in proteins compared to DNA. One reason for this limited knowledge is the heterogeneity of proteins and incomplete information about the protonation state of their ionizable residues, which are sensitive to the surrounding microenvironment. Similarly, little is known about how the long-range electrostatic interactions of protein and solution ions contribute to substrate binding and catalysis.

A recent study showed that a tyrosine residue deprotonates at high pH in the active site of the flavin-dependent nitronate monooxygenase from *Pseudomonas aeruginosa* PAO1 (PaNMO).[16] While the study demonstrated the presence of a tyrosinate at high pH, the enzyme contains four tyrosine residues in the active site, which made the system too cumbersome for further investigation. Here we study NADH:quinone oxidoreductase (NQO, EC 1.6.5.9, UniProtKB Q9I4 V0) from *P. aeruginosa* PAO1, an FMN-dependent enzyme that utilizes NADH to catalyze a two-electron reduction of quinones.[17] NQO has one ionizable tyrosine in the active site, making it possible to probe the effect of introducing a single, localized negative charge in the vicinity of the FMN cofactor.

NQO has been proposed to serve a dual function in the cell by preventing the formation of semiquinone radicals, which react with molecular oxygen to promote oxidative stress, and regenerating NADH for the catabolism of fatty acids.[18−20] Crystal structures of NQO at ≤2.2 Å resolution in both the free and NAD^+-bound forms showed the enzyme contains a TIM-barrel and an extended domain connected by two loops.[21,22] The tyrosine in the active site of NQO (Y277) has its hydroxyl O atom pointing toward the C_7 methyl group of the flavin with a separation of 3.0 Å (Figure 1).[21] In contrast with Y277, all other tyrosine residues in NQO are far from the FMN at a distance of ≥10 Å.

To probe the protonation state of the tyrosine and the electrostatic environment in the active site, we employ UV−visible absorption spectroscopy. The absorption spectrum of flavin is sensitive to the electrostatic microenvironment of the flavoprotein binding pocket[23] and varies in solvents of different polarity.[24−28] Changes in flavin absorption maxima have previously been observed upon the binding of negatively charged ligands.[29,30] However, studies with charged ligands could not disentangle the effects on the FMN absorption

Received: July 5, 2021
Accepted: August 23, 2021
Published: August 26, 2021

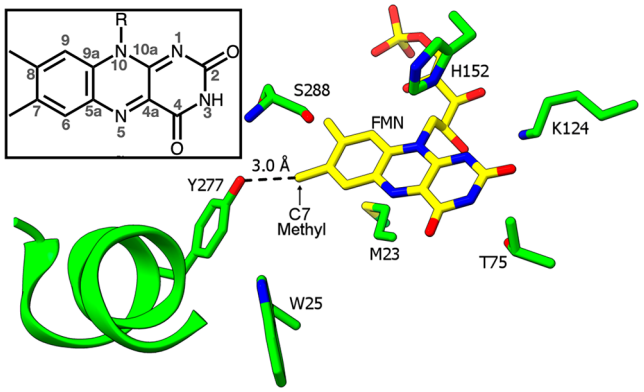

Figure 1. Active site of NQO depicting the positions of the FMN cofactor, key active site residues, and α helix where Y277 is anchored (PDB: 2GJL). The Y277 hydroxyl O atom is 3.0 Å from the flavin C_7 methyl C atom. Colors indicate FMN carbons (yellow), protein carbons and α helix (green), nitrogens (blue), and oxygens (red). The inset shows the structure of flavin with atom labels.

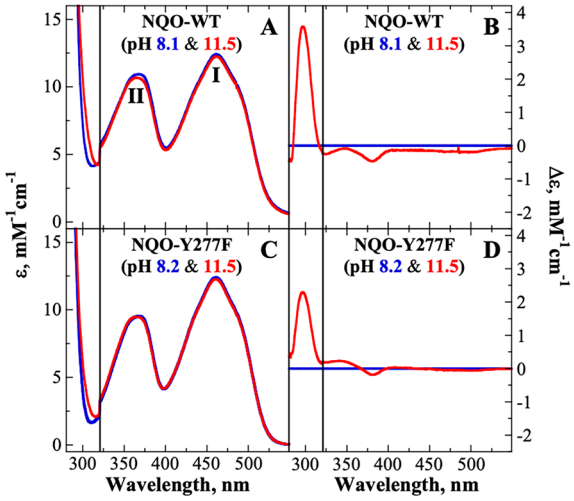

Figure 2. Absorption spectra for (A) NQO-WT and (C) NQO-Y277F are shown as pH increases from ~8.1 (blue) to 11.5 (red). Bands I and II are labeled in panel A. Difference absorption spectra for (B) NQO-WT and (D) NQO-Y277F are also shown where the spectra at pH ~8.1 was used as a baseline. Extinction coefficient values for the enzyme systems were corrected for the protein absorption (≥320 nm) by adjusting for flavin binding. The FMN/enzyme stoichiometry is 0.8 for NQO-WT and 0.7 for NQO-Y227F. Spectra were recorded in 10 mM NaP_i, 10 mM $NaPP_i$, 100 mM NaCl, and 20% glycerol at 15 °C.

spectrum from active site desolvation, protein−ligand hydrogen bonds and van der Waals interactions, and conformational changes that might result from the binding process.

It is expected that the deprotonation of a tyrosine (i.e., introducing a negative charge) in the NQO active site near FMN will perturb the UV−visible absorption spectrum of the FMN. This manuscript presents a joint computational and biochemical study in four parts; first, biochemical experiments indicate that Y277 deprotonates in NQO at high pH and that this deprotonation has a limited effect on the UV−visible absorption spectrum of FMN. Next, an initial set of computations show that introducing a negative charge at the position of Y277 should significantly perturb FMN's absorption spectrum. To explain this inconsistency, a second set of computations are presented incorporating solution ions that mimic the experimental concentration of salt used. The computations with solution ions agree with the biochemical experiments, suggesting that the solution ions mask the effect of the Y277 deprotonation on FMN's absorption spectrum. Lastly, preliminary biochemical experiments are presented to test this hypothesis, which indicate that solution ions play a role in perturbing absorption spectrum of protein-bound FMN without significantly altering the secondary structure of NQO.

To establish whether Y277 deprotonates to a tyrosinate at high pH *in vitro*, the ionizable hydroxyl group of Y277 was removed through a site-directed phenylalanine mutation (Y277F), and the UV−visible absorption spectra of NQO-WT and NQO-Y277F were compared at pH 8.1 and 11.5 (Figure 2). Upon increasing pH from 8.1 to 11.5, spectral changes at 295 nm were observed (Figure 2A), consistent with the deprotonation of tyrosine residues.[16,31,32] Specifically, ε_{295} increased by 3.5 mM^{-1} cm^{-1} when the pH increased from 8.1 to 11.5 (Figure 2B). When the titration was repeated for NQO-Y277F (Figure 2C), ε_{295} increased by 2.3 mM^{-1} cm^{-1} (Figure 2D). A plot of $\Delta\varepsilon_{295}$ as a function of pH yielded pK_a values of 10.7 ± 0.1 for NQO-WT and 10.6 ± 0.1 for NQO-Y277F (Figure 3A). The 1.2 mM^{-1} cm^{-1} difference in the $\Delta\varepsilon_{295}$ values and the comparable pK_a values estimated from the titrations with NQO-WT and NQO-Y277F indicated that Y277 is protonated at pH 8.1 and deprotonated in ~90% of the NQO-WT population at pH 11.5.

The titration was repeated for FMN in solution (free-FMN). As pH increases the N_3 atom of the FMN deprotonates, resulting in spectral changes seen in the difference spectrum (Figure 3B inset). No such spectral changes were observed for NQO-WT or NQO-Y277F (Figure 3B), indicating that the enzyme-bound flavin isoalloxazine remains neutral at pH 11.5. In agreement with previous studies, a pK_a value of 10.2 ± 0.1 was determined for FMN in bulk solvent by plotting the $\Delta\varepsilon_{489}$ values versus pH (Figure 3B).[23,33−36]

The maxima at ~360 nm (band II) and ~450 nm (band I) in Figure 2A are characteristic of FMN's absorption spectrum. The λ_{max} for bands I and II and ratio of band heights (intensities) are tabulated in Table 1. Surprisingly, while the difference spectra in Figure 2A show strong changes in the 295 nm range associated with deprotonation of Y277, minimal changes are observed in bands I and II associated with FMN, despite the introduction of a negative charge just 3.0 Å next to FMN. Computations are presented next to rationalize this observation.

Electrostatic spectral tuning maps (ESTMs) were prepared for lumiflavin, a minimal flavin model, to determine how negative point charges can modulate each excitation band in the flavin absorption spectrum.[24,37] The maps were prepared by placing a negative charge of $-0.1e$ at different positions on the flavin van der Waals surface and computing the flavin absorption spectrum in the presence of the point charge.[24,37] The van der Waals surface is then color coded according to the change. Specifically, for each of bands I and II, we report ESTMs for changes in absorption wavelengths (λ_I and λ_{II}) and changes in oscillator strengths (f_I and f_{II}), respectively (Figure 4). Oscillator strengths are correlated with band absorption intensity. See Experimental Methods for more details.

The maps in Figure 4 indicate that when a negative charge is placed near the flavin C_7 methyl group, a redshift in the band II maximum is expected (since the surface near the C_7 methyl

https://doi.org/10.1021/acs.jpclett.1c02173
J. Phys. Chem. Lett. 2021, 12, 8384−8396

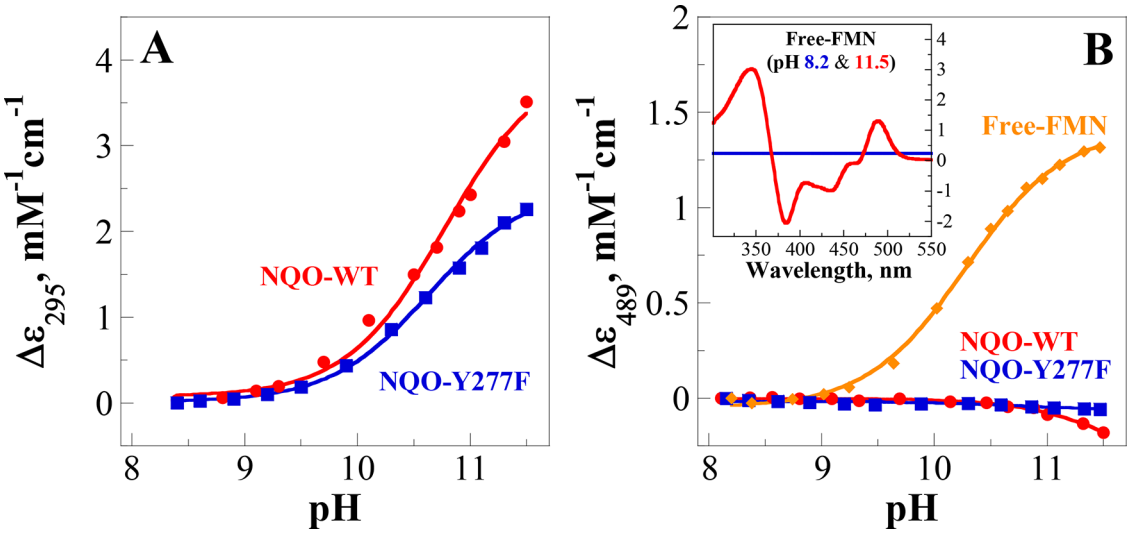

Figure 3. (A) Plot of $\Delta\varepsilon_{295}$ as a function of pH for NQO-WT (red) and NQO-Y277F (blue) to determine the pK_a of Y277. (B) Plot of $\Delta\varepsilon_{489}$ as a function of pH for free-FMN (orange), NQO-WT (red), and NQO-Y277F (blue). The inset shows difference absorption spectra for free-FMN at pH 11.5 relative to pH 8. Curves were fit to data points using eq 1. Data were obtained from spectra recorded in 10 mM NaP_i, 10 mM $NaPP_i$, 100 mM NaCl, and 20% glycerol at 15 °C.

Table 1. λ_{max} Values for FMN Bands I and II and Ratios of Intensities from Figure 2

	NQO-WT		NQO-Y277F	
	pH 8.1	pH 11.5	pH 8.2	pH 11.5
$\lambda_{band\ I}$ (nm)	461	461	460	460
$\lambda_{band\ II}$ (nm)	368	366	368	364
$\varepsilon_{band\ II/I}$	1.13	1.15	1.30	1.30

group in Figure 4 λ_{II} map is red). An increase in oscillator strength associated with band II is also expected, (blue color near C_7 in Figure 4 f_{II} map). In contrast, band I should undergo little to no redshift (Figure 4 λ_I) and a slight decrease in oscillator strength (Figure 4 f_I) when a negative charge is placed near the C_7 methyl group. These predictions are consistent with observations by Raffelberg et al. for spectral changes caused by mutations near flavin's C_7 methyl group in YtvA LOV from *Bacillus subtilis*.[38]

Clearly, none of the changes predicted from Figure 4 were observed experimentally upon Y277 deprotonation (Figure 2A). Delocalization of the negative charge in the tyrosinate aromatic ring may play a role, so excitation energies and oscillator strengths were also computed using tyrosine and tyrosinate point charges spatially placed to mimic the Y277−flavin arrangement in the crystal structure of NQO (figure not shown).[22] When tyrosine charges are replaced with tyrosinate charges, there is a 37% increase in f_{II}, a 6 nm red shift in λ_I, a 13% decrease in f_I, and a 14 nm red shift in λ_{II}. These results qualitatively agree with the tuning maps presented in Figure 4 and suggest that deprotonating a tyrosine close to the flavin C_7 methyl group would, *ceteris paribus*, significantly alter the flavin absorption spectrum.

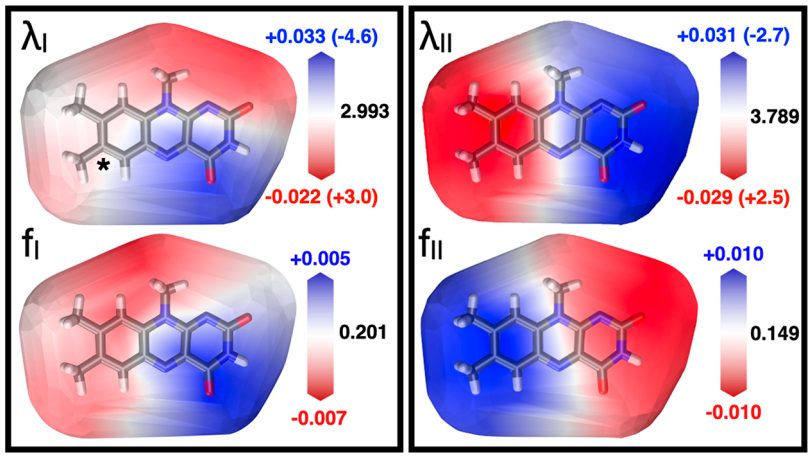

Figure 4. Electrostatic spectral tuning maps (from ref 37) and oscillator strength tuning maps (this work) demonstrate how a negative charge of −0.1*e* placed at various positions on the flavin van der Waals surface affect the absorption wavelengths (λ_I and λ_{II}) and oscillator strengths (f_I and f_{II}) for each of its absorption bands at 450 and 360 nm, respectively. The λ_I and λ_{II} map legends indicate the magnitude of the shifts relative to the gas-phase reference excitation energy in eV (nm in parentheses) caused by the −0.1e charge, while the f_I and f_{II} map legends indicate the change in the oscillator strength relative to the gas-phase reference strength. The approach to compute such maps is described in ref 18, using the B3LYP/6-31+G* method and basis set. The C_7 carbon is labeled with an asterisk in the λ_I map.

https://doi.org/10.1021/acs.jpclett.1c02173
J. Phys. Chem. Lett. 2021, 12, 8384−8396

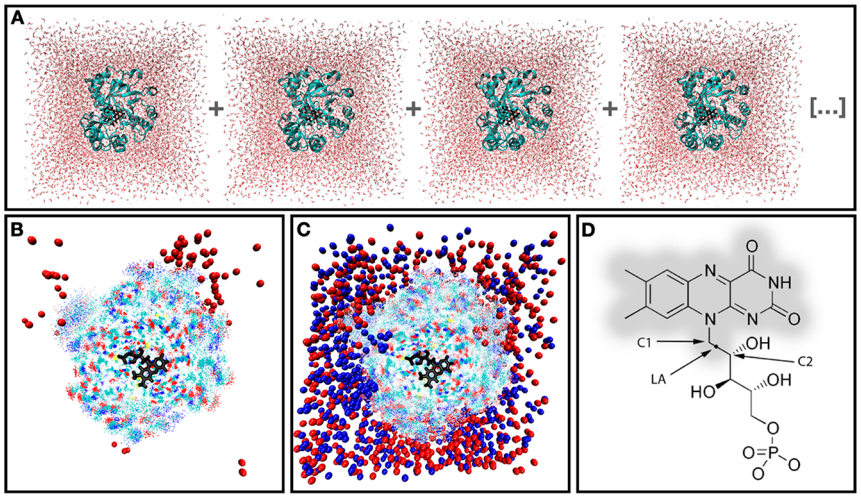

Figure 5. (A) Snapshots from a molecular dynamic simulation of NQO. A total of 100 such snapshots are used to generate the ASEC configuration shown in panel B. (B) Cross section of the ASEC configuration along the plane of the flavin isoalloxazine ring. The FMN is shown in black. Atoms of the protein sampled from 100 configurations are shown as points. 200 Cl^- pseudoions with $-0.01e$ charge are shown as red spheres. Not all 200 Cl^- pseudoions appear since this is a cross section showing only half of the system, and since some pseudoions are hidden behind the protein. Water molecules up to 30 Å from the flavin are included in the ASEC QM/MM calculations but are not shown here to allow visualization of the rest of the system. (C) The ASEC configuration for a system where 18 Na^+ and 20 Cl^- ions were added (1800 Na^+ pseudoions as blue spheres, 2000 Cl^- pseudoions as red spheres). See text for more details. (D) A scheme of the QM/MM frontier region. The lumiflavin (shaded region) is treated at the quantum mechanical (QM) level of theory, while the ribose-5′-phosphate group and the rest of the protein and solvent are described using a molecular mechanics (MM) force field.

Table 2. QM/MM Computed Oscillator Strengths and Excitation Wavelengths for Flavin Bands in NQO[a]

Y277 protonation state	oscillator strength (band I)	oscillator strength (band II)	wavelength, nm (band I)	wavelength, nm (band II)
protonated	0.087	0.270	428	361
unprotonated	0.057 (−35%)	0.322 (+19%)	434 (+6)	369 (+8)

[a]QM/MM (TD-B3LYP/aug-cc-pVDZ/AMBER) computed oscillator strengths and excitation wavelengths for the flavin absorption bands are shown. The numbers in parentheses indicate the % change in oscillator strength and the change in excitation wavelength in nm upon Y277 deprotonation. The QM/MM simulation space contained 2 Cl^- ions for the protonated model and 1 Cl^- ion from the unprotonated to neutralize the protein charges.

Reorientation of Y277 in the active site or local flexibility of nearby residues could explain the discrepancy between the experiments and the model calculations above. Therefore, the effect of Y277 deprotonation on the flavin absorption spectrum was evaluated *in silico* in the presence of the solvated protein structure using molecular dynamics (MD) followed by hybrid quantum mechanical/molecular mechanical (QM/MM) simulations on NQO with both protonated and unprotonated Y277. Specifically, the average solvent electrostatic configuration−free energy gradient (ASEC-FEG) approach is used for QM/MM.

The ASEC-FEG approach is described in more detail in the Experimental Methods. Briefly, the method allows the geometry optimization and property calculations of a molecule (here, the flavin group, described quantum mechanically) in the field of a time-averaged protein environment generated from molecular dynamics (MD). In this work, the ASEC configuration is generated by a superposition of 100 snapshots selected from a 500 ns MD trajectory (Figure 5A). The ASEC approach leaves the molecular mechanical representation of rigid atoms intact while replacing flexible atom point charges by a "cloud" of scaled charges with a Lennard-Jones potential that becomes wider and shallower with higher flexibility. If the QM system is polarized in the same way by the individual protein/solvent configurations, a single ASEC-FEG calculation would give a numerically identical result as averaging the QM/MM calculations for each configuration contributing to the ASEC. Therefore, the ASEC-FEG approach is particularly well suited for capturing an averaged long-range electrostatic interaction, as needed for this work.

ASEC-FEG combines the idea of the average solvent electrostatic configuration model,[39,40] originally developed to study molecular systems in solution, and the free energy gradient method proposed by Nagaoka et al.[41−43] ASEC-FEG has been extended to proteins by including van der Waals average interaction energy[44,45] and has recently been extended to model flavoproteins.[46] Therefore, the word "solvent" in ASEC really encompasses both the solvent and protein.

The protein model is constructed starting from the crystal structure of NQO (PDB: 2GJL). After assigning the amino acid protonation states, the protein has a total charge of +2, or +1 when Y277 is deprotonated; thus, the system is globally neutralized by adding 2 or 1 Cl^- ions, respectively. During the 500 ns MD, the O atom of Y277 remained around 3.2 Å away from the backbone of S288 irrespective of whether a tyrosine or tyrosinate was considered, likely due to a hydrogen bond interaction with the S288 backbone N atom. The ASEC-FEG configuration averaged 100 MD simulation frames to generate the QM/MM systems with tyrosine (Figure 5B) and tyrosinate. These ASEC configurations were then used to compute the TD-B3LYP/aug-cc-pVDZ excitation energies and oscillator strengths. The results qualitatively agree with the

https://doi.org/10.1021/acs.jpclett.1c02173
J. Phys. Chem. Lett. 2021, 12, 8384−8396

Table 3. Computed Oscillator Strengths and Excitation Wavelengths for Flavin Bands in NQO with Added Solution Ions[a]

Y277 protonation state	oscillator strength (band I)	oscillator strength (band II)	wavelength, nm (band I)	wavelength, nm (band II)
protonated	0.142	0.187	417	340
unprotonated	0.145 (+2%)	0.183 (−2%)	418 (+1)	339 (−1)

[a]QM/MM (TD-B3LYP/aug-cc-pVDZ/AMBER) computed oscillator strengths and excitation wavelengths for the flavin absorption bands in the presence of 18 added Na^+ and Cl^- ions. The numbers in parentheses indicate the % change in oscillator strength and the change in excitation wavelength in nm upon Y277 deprotonation.

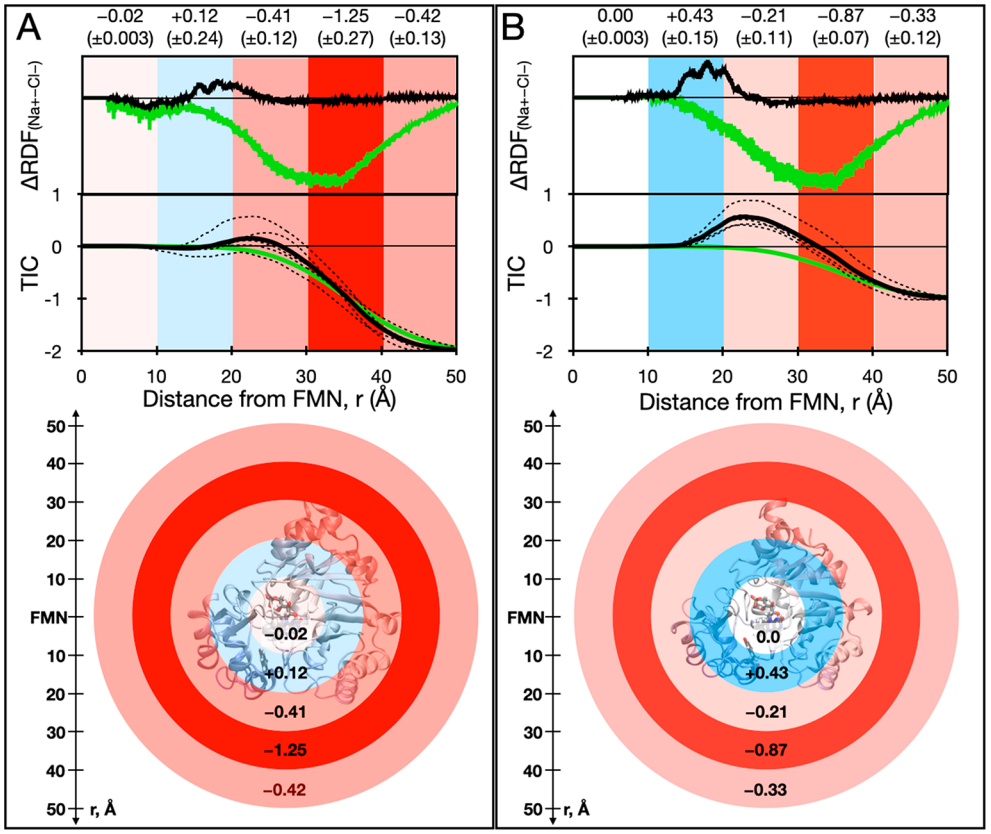

Figure 6. Top: The difference between the radial distribution functions (ΔRDF) of the Na^+ and Cl^- ions calculated for a 500 ns MD simulation of NQO-WT with (A) protonated and (B) deprotonated Y277. Simulations were run in the presence (black) and absence (green) of 18 added Na^+ and Cl^- ions. Below the ΔRDFs are plots of the corresponding total integrated charge (TIC, an integral of the RDF) as a function of distance for the full 500 ns trajectory (bold line) and for each 100 ns window (thin dashed lines). The numbers at the top indicate the total change in TIC for five shells around flavin, each 10 Å thick. The associated plus/minus uncertainty is the standard deviation calculated by averaging the result from five 100 ns windows (dashed lines). Bottom: The results for the 18 added Na^+ and Cl^- ions models are shown as the integrated RDFs for each shell up to 50 Å (i.e., the change in TIC for that shell) plotted on top of the protein structure, shown close to actual scale. The shading for each shell relates to the total charge within that spherical shell and should not be interpreted as suggesting an isotropic distribution of solution ions.

tuning maps carried out in the absence of the surrounding protein (Table 2).

Thus, using multiple computational methods and models, it is shown that Y277 deprotonation would yield a redshift of both flavin absorption bands, an increase in the oscillator strength at band II, and a decrease in the oscillator strength at band I.

So far, all the computational models are internally consistent but do not agree with the biochemical experiments presented at the start of this section. Interestingly, while the UV−visible absorption spectra for NQO-WT were acquired in a buffered solution with 100 mM NaCl, the QM/MM computations were carried out in a water solvent with 1−2 Cl^- ions, suggesting that solution ions might be the culprit for the differences between the *in vitro* and *in silico* results.

The 100 mM NaCl concentration from the biochemical experiment was mimicked *in silico* by adding 18 extra Na^+ and Cl^- ions to the simulation space and then repeating the MD and ASEC-FEG QM/MM calculations with both protonated and unprotonated Y277. The resulting ASEC is shown in Figure 5C for the protonated Y277 simulation, where the distribution of solution ions is visibly nonuniform and anisotropic. The corresponding ASEC-FEG QM/MM calculations predicted that deprotonating Y277 would yield negligible changes of 1 nm in absorption wavelength and 2% in absorption intensity at both flavin bands (Table 3). Thus, adding solution ions to the ASEC-FEG QM/MM models yielded results that agree with the biochemical experiment of Figure 2A.

The need for solution ions in the simulation suggests that the ions mask the effect of deprotonating Y277 on the flavin absorption spectrum. To help isolate the effect of the solution ions on the flavin (direct electrostatic effect vs indirectly by altering the conformational state of the protein), we repeat the

https://doi.org/10.1021/acs.jpclett.1c02173
J. Phys. Chem. Lett. 2021, 12, 8384−8396

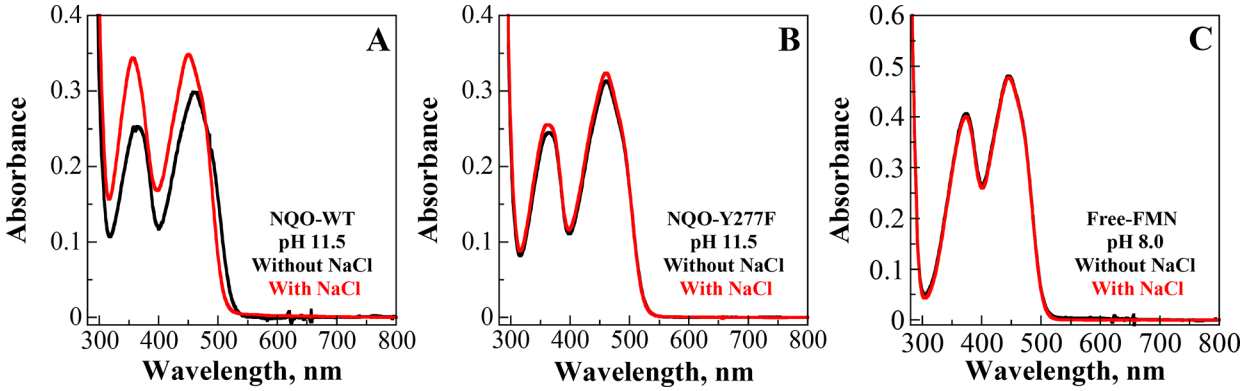

Figure 7. UV−visible absorption spectra of (A) NQO-WT at pH 11.5, (B) NQO-Y277F at pH 11.5, and (C) free-FMN at pH 8.0 in the absence (black) and presence (red) of 100 mM NaCl. Enzyme spectra were recorded in 50 mM piperidine at 10 °C, while the spectra with free-FMN were recorded in 10 mM HEPES at 10 °C. Spectra were recorded 2 min after the addition of NaCl, apart from NQO-WT at pH 11.5 which took an hour to equilibrate. Spectra are reported in absorbance instead of extinction coefficient values as the extinction coefficient values for all systems were previously reported in the presence of salt.

QM/MM calculations for the ASEC configuration keeping the system fixed (no MD resampling) and deleting the 18 added Na^+ and Cl^- ions from the unprotonated Y277 model, leaving only 2 Cl^- ions to keep the system neutral. Deleting the ions "unmasks" the effect of the tyrosinate (Table S1), resulting in redshifts of both bands and oscillator strength changes in agreement with the ESTMs in Figure 4 and the QM/MM calculations in Table 2.

To rule out that Na^+ ions enter the protein active site, we repeat the MD simulations with Na^+ ions initially planted near the Y277 tyrosinate. This computational experiment was repeated twice. After less than 1 ns, the Na^+ leaves the active site in both simulations.

The calculations indicate that the ions alter the flavin absorption spectrum through a long-range potential and suggest that the presence of the ions is responsible for the lack of an observed effect on the flavin's absorption spectrum when Y277 was deprotonated.

By comparing parts B and C of Figure 5, it may come as no surprise that solution ions affect the flavin absorption spectrum; the distribution of solution ions is anisotropic around the flavin particularly near the protein surface. However, Figure 5C shows only 100 snapshots and cannot easily be used to observe small rearrangements in the solution ions upon the deprotonation of Y277. To capture the change in ion distributions, we use radial distribution functions (RDFs). RDFs do not present the full picture, since they do not capture the anisotropy of the solution ions, but they adequately capture a rearrangement of the solution ions around the flavin center upon Y277 deprotonation.

RDFs were computed along the full 500 ns MD trajectory for both the protonated (black lines Figure 6A) and unprotonated (black lines Figure 6B) Y277 models with the 18 added Na^+ and Cl^- ions. Specifically, the differences in the RDFs (ΔRDF, computed using the Na^+ RDF minus the Cl^- RDF) and total integrated charge of the solution ions in the solvation sphere (TIC, see Experimental Methods) were plotted relative to the flavin center of mass (Figure 6). Plotting the RDFs and TICs relative to the Y277 O atom yielded qualitatively the same result. The bottom panels in Figure 6 uses colors to indicate the TIC in each 10 Å shell around the flavin center of mass. Upon deprotonating Y277, the charge density in the first 10 Å sphere around the flavin center of mass increased by just 0.02*e*, which suggests Na^+ ions rarely enter the active site pocket of NQO as a tyrosinate forms (Figure 6). In contrast, the positive charge density increased by over 0.20*e* in each 10 Å shell 10−40 Å from the flavin center of mass, indicating either that Na^+ ions moved closer to the protein surface and/or Cl^- ions moved away from the protein surface once Y277 is deprotonated (Figure 6). Therefore, while the model with Y277 in the anionic form contained one fewer Cl^- ion compared to the model with Y277 in the neutral form, the charge difference is not uniformly distributed with distance.

RDFs from MD simulations with only 1−2 Cl^- ions (green lines Figure 6) do not capture the redistribution of ions upon Y277 deprotonation, since Na^+ ions are missing. This explains why the 1−2 Cl^- ion models predicted that deprotonating Y277 would have a strong effect on the flavin absorption spectrum. On the other hand, the model with the added Na^+ ions shows a rearrangement of ions when Y277 deprotonates, such that the solvation shells near the protein surface become more positive; we hypothesize that the solution ions act as a long-range counterion to the Y277, largely canceling out its effect on FMN's absorption.

To ensure results of the RDFs are not due to a statistical anomaly, the TIC calculations for the entire 500 ns trajectory (Figure 6, bold lines) were compared for each 100 ns window within the full trajectory (Figure 6, thin dashed lines). These results consistently indicated that the density of Na^+ ions increases near the protein surface as Y277 deprotonates. However, the exact distribution of Na^+ ions is not fully consistent between the 100 ns windows, suggesting that longer MD simulations are required to obtain converged ionic distributions between windows.

Unlike QM/MM computations that can simulate Y277 deprotonation in a pure water solvent, the protein−cofactor complex is unstable in deionized water; thus, no experiment can closely mimic the fictional *in silico* system with 1−2 Cl^- ions. Instead, the experiments were repeated with minimal solution ions in the system by using piperidine as a bulky base with NQO-WT at pH 11.5. Piperidine, even in its conjugate acid form, is unlikely to occupy the same ionic distribution as monatomic ions such as Na^+. The UV−visible absorption spectrum of NQO-WT in the presence and absence of 100 mM NaCl was measured *in vitro* in 50 mM piperidine, at pH 11.5, to establish whether the addition of Na^+ and Cl^- ions

https://doi.org/10.1021/acs.jpclett.1c02173
J. Phys. Chem. Lett. 2021, 12, 8384−8396

Table 4. λ_{max} Values for FMN Bands I and II and Ratio of Intensities from Figure 7

	NQO-WT		NQO-Y277F		Free-FMN	
	no NaCl	with NaCl	no NaCl	with NaCl	no NaCl	with NaCl
$\lambda_{band\ I}$ (nm)	458	450	462	461	446	445
$\lambda_{band\ II}$ (nm)	364	356	364	363	374	374
$\varepsilon_{band\ II/I}$	1.18	1.01	1.28	1.27	1.19	1.18

Table 5. Steady-State Kinetics Parameters of NQO in the Presence and Absence of NaCl

kinetic parameter[a]	NQO-WT	NQO-WT + 100 mM NaCl	NQO-Y277F
k_{cat}, s^{-1}	13	5.2 (2.5× ↓)[b]	9 (1.4× ↓)[b]
$K_{m,NADH}$, μM	136	77 (1.8× ↓)	183 (1.3× ↑)
$K_{m,BQ}$, μM	17	7.5 (2.3× ↓)	7 (2.4× ↓)
$k_{cat}/K_{m,NADH}$, M^{-1} s^{-1}	94 000	70 000 (1.3× ↓)	50 000 (1.9× ↓)
$k_{cat}/K_{m,BQ}$, M^{-1} s^{-1}	750 000	720 000 (1.0× ↓)	1 300 000 (1.7× ↑)
R^2	0.987	0.992	0.939

[a]Kinetic parameters were determined in a solution of 50 mM piperidine, pH 11.5, either in the presence or absence of 100 mM NaCl at 25 °C. Standards errors were ≤18%. [b]The values in parentheses represent the change of the kinetic parameter with respect to NQO-WT in the absence of 100 mM NaCl, with ↓ representing a decrease and ↑ representing an increase.

would affect the flavin absorption spectrum in solution when Y277 is deprotonated.

In the absence of added NaCl, the UV−visible absorption spectrum of NQO-WT in aqueous piperidine had maxima at 364 and 458 nm (Figure 7A and Table 4). Upon the addition of 100 mM NaCl, both maxima blue-shifted by 8 nm, with a 26% increase in intensity at band II, and a 14% increase in intensity at band I (Figure 7A and Table 4). When KCl or KBr were used instead of NaCl, similar spectral changes were observed with an 8 nm blue shift at both bands, a ∼14% increase in the intensity at band II, and a ∼7% increase in intensity at band I, indicating that the observed effect is not exclusive to Na^+ and Cl^- ions (Figure S1). Addition of 100 mM NaCl to the NQO-Y277F mutant at pH 11.5 yielded no spectral changes (Figure 7B and Table 4), since, unlike NQO-WT at pH 11.5, there is no charged residues in the active site of this mutant. Similarly, when 100 mM NaCl was added to flavin in bulk solution at pH 8.0, no changes in the flavin bands were observed (Figure 7C and Table 4).

If NaCl ions help to mask the interaction between unprotonated Y277 and the flavin, the addition of these ions should have a qualitatively opposite effect relative to the computationally predicted effect of the deprotonated tyrosinate. Indeed, the observed blue shifts at both flavin bands and the increase in intensity at band I after addition of NaCl to NQO-WT at pH 11.5 (Figure 7A) would mostly cancel out the computationally predicted effect of the tyrosine deprotonation on the flavin absorption spectrum (Table 2).

The spectroscopic measurements in piperidine demonstrate that adding solution ions has a direct effect on the NQO-WT absorption spectrum, but do not rule out the possibility that the protein undergoes denaturation or a large conformational change upon salt addition. Therefore, we determined the effect of adding 100 mM NaCl on the enzymatic activity of NQO. The steady-state kinetic parameters of NQO-WT were determined with 1,4-benzoquinone and NADH in the presence and absence of 100 mM NaCl at pH 11.5 and 25 °C. The best fit of the kinetic data was obtained with an equation describing a ping-pong Bi−Bi steady-state kinetic mechanism, in agreement with previous studies on NQO-WT at pH 7.4.[17] As shown in Table 5, the k_{cat}, $K_{m,NADH}$, $K_{m,BQ}$, $k_{cat}/K_{m,NADH}$, and $k_{cat}/K_{m,BQ}$ values exhibited a ≤2.5-fold difference between the presence and absence of 100 mM NaCl. This indicates that solution ions have a minimal effect on substrate binding and enzyme catalysis, and therefore that the structure of the enzyme and topology of the active site residues are not strongly perturbed by the presence of added salt. Similar ≤2.5-fold differences in the steady-state kinetic parameters were observed when NQO-Y277F was compared to NQO-WT at pH 11.5 in the absence of 100 mM NaCl (Table 5), indicating that mutating Y277 to a phenylalanine has a minimal effect on the structure and active site topology of the enzyme and that Y277 does not directly participate in substrate binding and catalysis.

Overall, the steady-state kinetics suggest that NQO is stable following the deprotonation of Y277 and addition of solution ions. This rules out major conformational changes of the protein for which significantly different kinetic parameters would be expected.

In conclusion, in this work, we focus on NQO, a flavin enzyme that is conveniently structurally stable to changes in pH and ionic strength. The enzyme also conveniently hosts a single tyrosine residue (Y277) near the FMN that is 90% deprotonated at pH 11.5. In this model system, we investigate the effect of deprotonating Y277 on the flavin UV−visible absorption spectrum. Surprisingly, the deprotonation of Y277 is found to have little to no effect on the flavin absorption spectrum. Computations suggest that solution ions rearrange upon Y277 deprotonation, countering the effect of the Y277 tyrosinate on the absorption spectrum of FMN.

There is limited knowledge of the relative contributions of short-range and long-range electrostatics to the potential acting on an active site in proteins. In discussions of spectral tuning of biological chromophores, most studies emphasize how polar or charged active-site residues tune the absorption wavelength. Often neglected in these discussions, however, is how collective long-range electrostatics from many charged species (surface residues and nearby solution ions) also alter the absorption wavelength and other biophysical properties of a chromophore or cofactor.

The importance of solution ion placement in QM/MM simulations has been described in other systems, such as in rhodopsins.[47−49] Similarly, the effect of solvent long-range electrostatics has also been emphasized, for instance, in the

https://doi.org/10.1021/acs.jpclett.1c02173
J. Phys. Chem. Lett. 2021, 12, 8384−8396

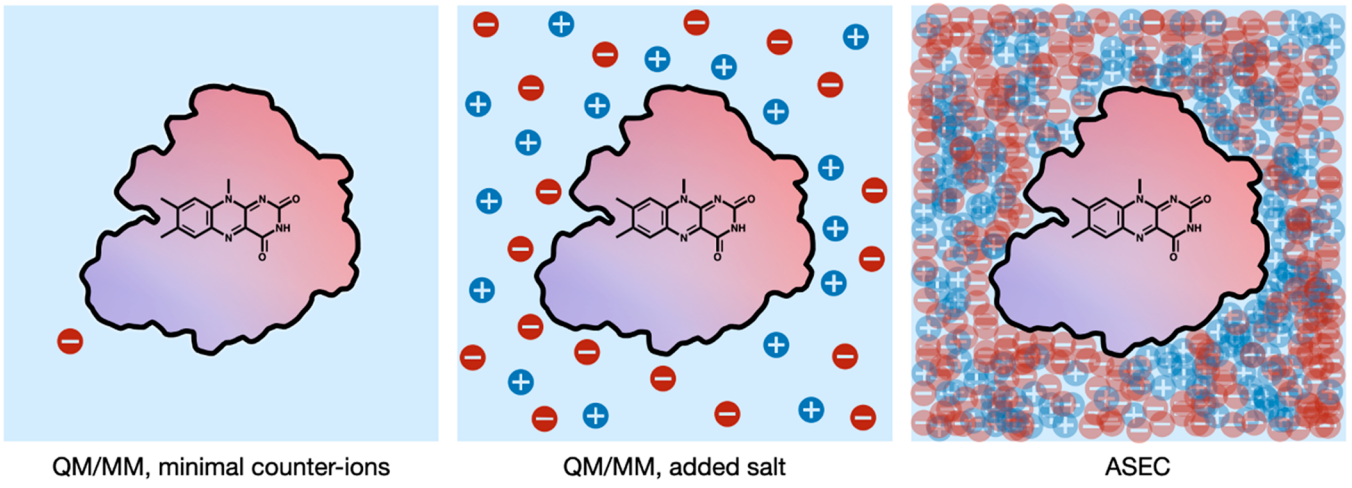

Figure 8. Schematic representation of computational models for including solution ions. The black outline represents the protein surface, while the blue and red gradient schematically represent surface regions of the protein with different charges. The blue and red spheres represent positively and negatively charged monatomic solution ions, respectively. (A) The commonly used minimal ions model. (B) The extra ions model where ions are added to mimic the concentration of salts in biochemical solutions. The frame only captures one distribution of ions surrounding the protein. (C) The ASEC model, which averages the interaction potential between the QM subsystem and the solution ions.

calculation of redox potentials.[50−53] The current study also establishes the importance of properly modeling solution ions, which are often overlooked, to accurately simulate the electrostatic environment of a solvated protein active site.

During the construction of QM/MM models, it is common practice to simply add a few counterions to neutralize protein charges and keep the system globally neutral (Figure 8A); however, this methodology could miss important contributions of solution ions, resulting in incorrect computational predictions (as demonstrated by the disparity in results between Table 2 and Figure 2A). More accurate models may include multiple positive and negative solution ions in the simulation space (Figure 8B). However, a single solvated QM/MM model cannot capture a thermodynamic ensemble that samples the many positions solution ions can take, and the result of the QM/MM calculations will likely depend on the ion placement. The ASEC-FEG approach is particularly well suited to address this problem; long-range interactions with individual ions are replaced by interactions with many pseudoions with scaled charges (Figure 8C). The positions of the ions originate from a MD simulation, to represent the distribution of the ions surrounding the protein. Due to ergodicity, the time-averaged potential felt by the flavin in the QM subsystem in ASEC is representative of the average potential experienced by many flavin molecules in a thermodynamic ensemble.

When ASEC-FEG QM/MM computations were carried out in the presence of both Na^+ and Cl^- solution ions, the results were consistent with the biochemical study, yielding no change in the flavin bands upon deprotonating Y277. Analyzing the distribution of the ions from the MD and ASEC-FEG simulations established that the solution ions rearranged to increase the positive charge density surrounding the protein surface as Y277 becomes deprotonated.

Preliminary biochemical experiments, where piperidine is used in the place of an ionic base and NaCl is later added, resulted in FMN spectral changes consistent with a masking of the computationally predicted effect of the tyrosinate. The different conditions used in this experiment compared to the first experiments discussed in this work makes it difficult to disentangle the effects of the solution ions, piperidine, and conformational effects of the protein on the FMN absorption spectrum, although kinetic experiments indicate that the protein does not undergo major structural changes upon addition of NaCl. Still, while the computations can be used to extract a single phenomenon (long-range electrostatics due to solution ions), computational and biochemical experiments to further investigate this system is left to future work.

Debye and Hückel have demonstrated that the mean mutual distance between solution ions modulates the energy and properties of an ionic solution.[54] The rearrangement of ions observed here in response to the appearance of an embedded charge within the protein binding site is reminiscent of the "ionic atmosphere" in the Debye−Hückel theory. Just as in Debye and Hückel's theory, this ionic distribution and redistribution in response to a perturbation should influence the energies and properties of the protein and its cofactor(s). It is likely that the electrostatic interactions with nonuniformly distributed solution ions affects other biophysical properties of the protein, not just the cofactor's absorption spectrum. The results in the current study are a reminder not the overlook solution ions when developing experiments and theories that evaluate protein biophysical properties.

EXPERIMENTAL METHODS

Materials. A QIAprep Spin Miniprep Kit was purchased from Qiagen (Valencia, CA). Isopropyl-1-thiol-β-D-galactopyranoside (IPTG) was ordered from Promega (Madison, WI). *Escherichia coli* strains DH5α and Rosetta(DE3)pLysS were purchased from Invitrogen Life Technologies (Grand Island, NY) and Novagen (Madison, WI), respectively. HiTrapTM chelating HP 5 mL affinity column and prepacked PD-10 desalting columns were purchased from GE Healthcare (Piscataway, NJ). Riboflavin 5′ phosphate sodium salt was purchased from MP Biomedicals LLC (Solon, OH). All other reagents used were of the highest purity commercially available.

Enzyme Preparation. The synthesis and cloning in a pET20b(+) plasmid for NQO variant Y277F was prepared by Genescript (Piscataway, NJ). The mutant gene was

https://doi.org/10.1021/acs.jpclett.1c02173
J. Phys. Chem. Lett. 2021, 12, 8384−8396

sequenced by Macrogen Inc. (Rockville, MD). Plasmids were purified using the Qiagen QIAquick Spin Miniprep Kit according to the manufacturer's protocol. The purified plasmids were transformed into chemically competent *E. coli* strain DH5α and Rosetta(DE3)pLysS cells using the heat shock method.[55] NQO-Y277F was expressed in *E. coli* strain Rosetta(DE3)pLysS and purified using methods previously described for NQO-WT.[17] Purified NQO-WT and NQO-Y277F were stored at −20 °C in 20 mM NaP_i, pH 8.0, 100 mM NaCl, and 10% glycerol. The total protein concentration was determined using the Bradford method.[56]

UV−Visible Absorption Spectroscopy. UV−visible absorption spectra were recorded using an Agilent Technologies model HP 8453 PC diode-array spectrophotometer (Santa Clara, CA) equipped with a thermostated water bath. The UV−visible absorption spectra of NQO-WT, NQO-Y277F, and free-FMN were determined as a function of pH in 10 mM NaP_i, 10 mM $NaPP_i$, 100 mM NaCl, and 20% glycerol, where enzyme storage buffers were exchanged using a PD-10 desalting column prior to use. Each 2.5 mL buffered solution was subjected to 1−10 μL serial additions of 1 M NaOH using a 10 μL syringe while the solution was stirring. Absorption spectra were incrementally taken at 15 °C as pH increased from 8.1 to 11.5. After each addition of base, the system was allowed to equilibrate until no changes in the pH value and absorption spectrum were observed, which typically required 1−2 min. Resulting spectra were corrected for absorbance at 800 nm and the dilution factor by the addition of NaOH. For enzyme solutions, the spectra were corrected for concentration using ε_{461} = 12 400 $M^{-1}cm^{-1}$ for NQO-WT[17] and ε_{461} = 12 000 $M^{-1}cm^{-1}$ for NQO-Y277F (this study). The extinction coefficient of NQO-Y277F was determined under the same conditions as NQO-WT by extracting the flavin cofactor through heat denaturation in 20 mM KP_i, pH 7.0, and 200 mM NaCl at 25 °C.[57]

The effect of NaCl on the flavin absorption spectra was determined for NQO-WT, NQO-Y277F, and free-FMN. NQO-WT and NQO-Y277F were prepared in a 50 mM piperidine solution at pH 11.5 using a PD-10 desalting column, while free-FMN was prepared in 10 mM HEPES at pH 8.0. After collecting 1 mL of each solution, an absorption spectrum was immediately taken at 10 °C with air blowing toward the cuvette to prevent moisture condensation. Following the initial spectrum, NaCl was added to a final concentration of 100 mM, and spectra were taken at 10 min intervals up to an hour. Each absorption spectrum took ∼5 min to equilibrate following the addition of NaCl except for NQO-WT at pH 11.5, which took an hour to equilibrate.

Steady-State Kinetics. Enzymatic activity was measured using an Agilent Technologies model HP 8453 PC diode-array spectrophotometer equipped with a thermostated water bath. The steady-state kinetic parameters for NQO-WT and NQO-Y277F were measured using the method of initial rates with varying concentrations of the substrates NADH and 1,4-benzoquinone.[58] Stock solutions of 1,4-benzoquinone were prepared in 100% ethanol. The effect of ethanol on enzyme activity was minimized by ensuring the final concentration of ethanol in the assay reaction mixture was at 1%. The enzymatic activity of NQO-WT and NQO-Y277F was determined in 50 mM piperidine at pH 11.5 and 25 °C. Additionally, the effect of NaCl on the kinetic parameters of NQO-WT was determined in a solution containing 50 mM piperidine, pH 11.5, and 100 mM NaCl at 25 °C. Reaction rates for NQO-WT were measured by following NADH consumption at 340 nm using ε_{340} = 6220 $M^{-1}cm^{-1}$ with a final enzyme concentration of 100 nM. For NQO-Y277F, the consumption of NADH was monitored at 368 nm using ε_{368} = 2770 $M^{-1}cm^{-1}$ with a final enzyme concentration of 200 nM.

Data Analysis. All experimental data were fit to equations using the KaleidaGraph software (Synergy Software, Reading, PA). The effect of pH on the UV−visible absorption spectrum of NQO-WT, NQO-Y277F, and free-FMN was fit to eq 1, which describes a curve with one pK_a value and two limiting values at high pH (A) and low pH (B). The kinetic data determined from initial rates using varying concentrations of NADH and 1,4-benzoquinone was fit to eq 2, which describes a ping-pong Bi−Bi steady-state kinetic mechanism with no inhibition by either substrate; here, v_o represents the initial rate of reaction, e is the concentration of enzyme, k_{cat} is the maximum rate of enzyme turnover at saturating concentrations of both NADH and 1,4-benzoquinone, and K_{NADH} and K_{BQ} are the Michaelis constants for NADH and 1,4-benzoquinone, respectively.

$$Y = \frac{A + B \times 10^{(pK_a - pH)}}{1 + 10^{(pK_a - pH)}} \quad (1)$$

$$\frac{v_0}{e} = \frac{k_{cat}[NADH][BQ]}{K_{NADH}[BQ] + K_{BQ}[NADH] + [NADH][BQ]} \quad (2)$$

Electrostatic Spectral Tuning Maps. ESTMs (λ_1 and λ_2 in Figure 4) were computed for lumiflavin at the B3LYP/6-31+G* level of theory in an earlier study.[37] Note that the color scheme here is inverted with respect to refs 37 and 24 since the ESTMs in this work indicate the effect of a negative charge on absorption wavelength as opposed to a positive charge as was the case in earlier studies. This study also reports oscillator strength tuning maps (f_1 and f_2 in Figure 4), which are computed using the same protocol as described in ref 37 but visualizing the oscillator strength changes instead of absorption wavelengths.

ASEC-FEG Calculations. The ASEC-FEG method and theory have been previously described largely for molecules in solution[39,40] and for retinal proteins.[44,45] However, we briefly describe the theory and the methodology as applied here to flavoproteins. Overall, the goal of ASEC is to account for sampling of the protein and solvent environment without substantially increasing the computational cost of QM/MM calculations.

Within the additive QM/MM scheme, the average of the total QM/MM energy $\langle E_{Total} \rangle$ is computed using

$$\langle E_{Total} \rangle = \langle E_{QM} \rangle + \langle E_{MM} \rangle + \langle E_{interaction} \rangle \quad (3)$$

The angle brackets indicate an average over an ensemble, which may be generated by MD or Monte Carlo simulations. The above separation of terms is valid for a system where the QM subsystem is not strongly differentially polarized by the different MM configurations. For a conformationally rigid QM subsystem, such as the flavin isoalloxazine moiety, the QM energy of a representative QM/MM structure is a good approximation to $\langle E_{QM} \rangle$. How to obtain such a representative QM structure is discussed after a few paragraphs.

It is possible to sample the protein environment around the flavin structure by freezing the QM atom coordinates and performing an MD simulation of all other atoms (protein and solvent). The average interaction energy is then obtained as

https://doi.org/10.1021/acs.jpclett.1c02173
J. Phys. Chem. Lett. 2021, 12, 8384−8396

the average of several QM/MM snapshots. Alternatively, since the $E_{interaction}$ terms are additive, one single QM/MM calculation could be performed in an MM environment that is a superposition of several protein configurations (see Figure 5B). Namely, the Lennard-Jones potential (E_{LJ}) and electrostatic potential ($E_{Electrostatic}$) experienced by the QM subsystem is an average one,

$$\langle E_{interaction} \rangle = \langle E_{electrostatic} \rangle + \langle E_{LJ} \rangle \quad (4)$$

$$\langle E_{electrostatic} \rangle = \sum_{i}^{n} \sum_{j}^{m} \sum_{k}^{l} \frac{q_i q_j / l}{r_{ij}^{k}} \quad (5)$$

$$\langle E_{LJ} \rangle = \sum_{i}^{n} \sum_{j}^{m} \sum_{k}^{l} 4\sqrt{\varepsilon_i \frac{\varepsilon_j}{l^2}} \left[\left(\frac{\sigma_{ij}}{r_{ij}^{k}} \right)^{12} - \left(\frac{\sigma_{ij}}{r_{ij}^{k}} \right)^{6} \right] \quad (6)$$

where i is an index over n QM atoms, j is an index over m MM atoms, and k is an index for the distance r over l uncorrelated configurations obtained from MD simulations. In this work, we use 100 configurations selected at regular time intervals from a 500 ns molecular dynamics simulation; The charge and van der Waals parameters of these 100 configurations are scaled accordingly, using $l = 100$ in eqs 5 and 6.

The optimization of a "representative" geometry of the QM subsystem for the $\langle E_{QM} \rangle$ term in eq 3 is done self-consistently. Namely, an initial geometry is used to generate an ASEC environment following an MD simulation with a frozen QM subsystem, and the QM subsystem is then optimized in the field of the frozen ASEC MM environment. The optimized QM structure and updated charges, computed using the electrostatic potential fitted (ESPF) approach,[59] are used to update the ASEC environment. This process is repeated until geometry convergence (i.e., until the energy difference relative to the previous step is less than a threshold of 0.5 kcal/mol).

The second term in eq 3, $\langle E_{MM} \rangle$, cancels out in the calculation of vertical excitation energies and is therefore not considered.

During the QM/MM calculations, the protein is divided into two subsystems: (i) the QM region, comprising the lumiflavin shown in Figure 5D, and (ii) the MM region, which includes all other atoms in the simulation (the ribose-5′-phosphate group, the protein, the solvent, and solution ions). The frontier between the QM and the MM parts is treated using the link atom (LA) approach.[60] The LA position is restrained using the Morokuma scheme.[61] The LA separates the lumiflavin, which is neutral, from the ribose-5′-phosphate group. The phosphate is predominantly deprotonated in the 8−11.5 pH range used in this study, and therefore, it has a charge of −2 in the simulations. The MM atom closest to the LA (C2 in Figure 5D) has its charge set to zero to avoid overpolarizing the QM/MM frontier.

Prior to MD simulations used to generate ASEC configurations, NQO was solvated in a 70 AÅ cubic water box. MD simulations were carried out using the GROMACS code.[62] AMBER99sb,[63] and TIP3P[64] force fields were used for the protein and water molecules, respectively. An initial pre-equilibration of the entire system was performed in the *NPT* ensemble by heating the system from 0 to 300 K in 300 ps, followed by 1000 ps of equilibration. Next, MD in the *NVT* ensemble was performed using 5000 ps for thermalization and 500 ns for production under standard ambient temperature and pressure. Periodic boundary conditions (PBC) were used to avoid boundary effects, and the particle-mesh Ewald method was used for computing long-range interactions.[65] In order to neutralize the total positive charge of NQO, Cl^- ions were added to the solvent box using "genion" in GROMACS.

MD and ASEC-FEG calculations were performed for NQO-WT with a standard Y277 and a deprotonated Y277. For the latter, the parameters for the tyrosinate were obtained from the Automated Force Field Topology Builder (ATB) repository.[66]

For geometry optimizations, the QM subsystem is treated at the complete-active-space self-consistent field (CASSCF) level of theory[67] and the ANO-L-VDZP basis set.[68] The active space used is 16 electrons and 14 orbitals, which includes all the π-electron system excluding one π and π^* orbital. The ASEC configuration used in the QM calculations comprises the protein, all solution ions, and solvent atoms within 30 Å from the flavin molecule. This choice for the solvent is assumed to be a better compromise than using a cubic system to avoid nonsymmetric effects in the absence of periodic boundary conditions.

The converged optimized structure is used to compute the oscillator strength and excitation energy of the system. For consistency with the ESTMs, which were generated using time-dependent density functional theory (TD-DFT) with B3LYP exchange, spectral shifts and oscillator strengths were computed using TD-B3LYP/aug-cc-pVDZ.

A few other methods and basis sets were tested for the ASEC QM/MM calculations. Specifically, geometry optimization of the system using B3LYP and using a Pople basis set followed by TD-DFT at the same level of theory yielded similar results to the CASSCF-optimized calculations. Spectral shifts and strengths were also computed using the multistate complete active space second-order perturbation theory (MS-CASPT2)[69] with the ANO-L-VDZP basis set. However, due to the dependence of the absolute MS-CASPT2 results on choice of active space, state averaging, and use of length vs velocity gauge[70] for oscillator strength calculations in this system, we focus on the TD-DFT results in this manuscript. The MS-CASPT2 calculations lead to the same conclusions as the B3LYP results, regardless of the details of the state-averaging and gauge used, and the discussions in this study remain true for all control calculations performed. We note that TD-DFT with B3LYP exchange has been successfully used to simulate UV−visible and FTIR spectra of flavin in good agreement with experiments in prior studies.[24,71−75]

All the multiconfigurational QM/MM calculations were computed with the OpenMolcas-TINKER interface.[76,77] TD-DFT calculations in the presence of ASEC point charges were performed in Gaussian 03.[78]

To study the effect of solution ions, 18 pairs of Na^+ and Cl^- ions (1 NaCl per 555 water molecules, equivalent to a ca. 100 mM NaCl solution) were added to the solvent box in addition to the Cl^- ions originally needed to neutralize the system, and molecular dynamics simulations were repeated using the same conditions.

Radial Distribution Functions (RDFs). RDFs were computed with the periodic boundary conditions using the *gmx rdf* tool in GROMACS. The total integrated charge (TIC) is computed from the difference in the cumulative number RDF (also sometimes called the "coordination number") of the Na^+ and Cl^- ions.

https://doi.org/10.1021/acs.jpclett.1c02173
J. Phys. Chem. Lett. 2021, 12, 8384−8396

■ ASSOCIATED CONTENT

Supporting Information

The Supporting Information is available free of charge at https://pubs.acs.org/doi/10.1021/acs.jpclett.1c02173.

QM/MM computed changes in flavin oscillator strengths and excitation wavelengths from protonated Y277 with 18 added Na^+ and Cl^- ions to unprotonated Y277 with the added solution ions removed from the simulation space (Table S1) and the UV−visible absorption spectrum for NQO-WT in 50 mM piperidine, pH 11.5, in the presence and absence of 100 mM KCl or KBr (Figure S1) (PDF)

■ AUTHOR INFORMATION

Corresponding Authors

Giovanni Gadda − *Department of Chemistry, Georgia State University, Atlanta, Georgia 30302, United States; Department of Biology and Center for Diagnostics and Therapeutics, Georgia State University, Atlanta, Georgia 30302, United States;* orcid.org/0000-0002-7508-4195; Email: sgozem@gsu.edu

Samer Gozem − *Department of Chemistry, Georgia State University, Atlanta, Georgia 30302, United States;* orcid.org/0000-0002-6429-2853; Email: ggadda@gsu.edu

Authors

Benjamin D. Dratch − *Department of Chemistry, Georgia State University, Atlanta, Georgia 30302, United States*

Yoelvis Orozco-Gonzalez − *Department of Chemistry, Georgia State University, Atlanta, Georgia 30302, United States;* orcid.org/0000-0001-7225-2424

Complete contact information is available at: https://pubs.acs.org/10.1021/acs.jpclett.1c02173

Author Contributions

B.D.D. and Y.O.-G. contributed equally to this work. B.D.D. and G.G. designed the biochemical experiments. Y.O.-G. and S.G. designed the computational experiments. B.D.D. conducted the purification, UV−visible absorption, and steady-state kinetic experiments. Y.O.-G. produced the ESTMs, MD, ASEC-QM/MM, and RDF calculations. B.D.D., Y.O.-G., G.G., and S.G. contributed to analyzing the results and writing the paper. G.G. and S.G. supervised the research.

Notes

The authors declare no competing financial interest.

■ ACKNOWLEDGMENTS

We are grateful to Dr. Donald Hamelberg for comments and discussions related to this work. The authors would also like to thank the anonymous reviewers for their constructive comments. This material is based upon work supported by the National Science Foundation (NSF) under Grant Nos. CHE-2047667 and CHE-1506518. We acknowledge the NSF XSEDE for computational resources through Research Allocation CHE180027. We also acknowledge the Advanced Research Computing Technology and Innovation Core (ARCTIC) resources, which are supported by the NSF Major Research Instrumentation (MRI) Grant Number CNS-1920024.

■ REFERENCES

(1) Barroso da Silva, F. L.; Derreumaux, P.; Pasquali, S. Protein-Rna Complexation Driven by the Charge Regulation Mechanism. *Biochem. Biophys. Res. Commun.* **2018**, *498*, 264−273.

(2) Dickey, A.; Faller, R. Examining the Contributions of Lipid Shape and Headgroup Charge on Bilayer Behavior. *Biophys. J.* **2008**, *95*, 2636−46.

(3) Draper, D. E. A Guide to Ions and Rna Structure. *RNA* **2004**, *10*, 335−43.

(4) Gitlin, I.; Carbeck, J. D.; Whitesides, G. M. Why Are Proteins Charged? Networks of Charge-Charge Interactions in Proteins Measured by Charge Ladders and Capillary Electrophoresis. *Angew. Chem., Int. Ed.* **2006**, *45*, 3022−60.

(5) Lee, A. G. How Lipids Affect the Activities of Integral Membrane Proteins. *Biochim. Biophys. Acta, Biomembr.* **2004**, *1666*, 62−87.

(6) Gadda, G. Oxygen Activation in Flavoprotein Oxidases: The Importance of Being Positive. *Biochemistry* **2012**, *51*, 2662−2669.

(7) Harris, T. K.; Turner, G. J. Structural Basis of Perturbed Pka Values of Catalytic Groups in Enzyme Active Sites. *IUBMB Life* **2002**, *53*, 85−98.

(8) Liu, Y.; Thoden, J. B.; Kim, J.; Berger, E.; Gulick, A. M.; Ruzicka, F. J.; Holden, H. M.; Frey, P. A. Mechanistic Roles of Tyrosine 149 and Serine 124 in Udp-Galactose 4-Epimerase from Escherichia Coli. *Biochemistry* **1997**, *36*, 10675−10684.

(9) Gribenko, A. V.; Patel, M. M.; Liu, J.; McCallum, S. A.; Wang, C.; Makhatadze, G. I. Rational Stabilization of Enzymes by Computational Redesign of Surface Charge−Charge Interactions. *Proc. Natl. Acad. Sci. U. S. A.* **2009**, *106*, 2601.

(10) Sanchez-Ruiz, J. M.; Makhatadze, G. I. To Charge or Not to Charge? *Trends Biotechnol.* **2001**, *19*, 132−135.

(11) Feig, M.; Pettitt, B. M. Sodium and Chlorine Ions as Part of the DNA Solvation Shell. *Biophys. J.* **1999**, *77*, 1769−1781.

(12) Owczarzy, R.; You, Y.; Moreira, B. G.; Manthey, J. A.; Huang, L.; Behlke, M. A.; Walder, J. A. Effects of Sodium Ions on DNA Duplex Oligomers: Improved Predictions of Melting Temperatures. *Biochemistry* **2004**, *43*, 3537−3554.

(13) Rubinstein, A.; Sherman, S. Influence of the Solvent Structure on the Electrostatic Interactions in Proteins. *Biophys. J.* **2004**, *87*, 1544−57.

(14) Hud, N. V.; Plavec, J. A Unified Model for the Origin of DNA Sequence-Directed Curvature. *Biopolymers* **2003**, *69*, 144−158.

(15) Maffeo, C.; Yoo, J.; Comer, J.; Wells, D. B.; Luan, B.; Aksimentiev, A. Close Encounters with DNA. *J. Phys.: Condens. Matter* **2014**, *26*, 413101−413102.

(16) Su, D.; Aguillon, C.; Gadda, G. Characterization of Conserved Active Site Residues in Class I Nitronate Monooxygenase. *Arch. Biochem. Biophys.* **2019**, *672*, 108058.

(17) Ball, J.; Salvi, F.; Gadda, G. Functional Annotation of a Presumed Nitronate Monoxygenase Reveals a New Class of Nadh:Quinone Reductases. *J. Biol. Chem.* **2016**, *291*, 21160−21170.

(18) Deller, S.; Macheroux, P.; Sollner, S. Flavin-Dependent Quinone Reductases. *Cell. Mol. Life Sci.* **2008**, *65*, 141.

(19) Ezraty, B.; Gennaris, A.; Barras, F.; Collet, J.-F. Oxidative Stress, Protein Damage and Repair in Bacteria. *Nat. Rev. Microbiol.* **2017**, *15*, 385.

(20) Iyanagi, T.; Yamazaki, I. One-Electron-Transfer Reactions in Biochemical Systems V. Difference in the Mechanism of Quinone Reduction by the Nadh Dehydrogenase and the Nad(P)H Dehydrogenase (Dt-Diaphorase). *Biochim. Biophys. Acta, Bioenerg.* **1970**, *216*, 282−294.

(21) Ball, J.; Reis, R. A. G.; Agniswamy, J.; Weber, I. T.; Gadda, G. Steric Hindrance Controls Pyridine Nucleotide Specificity of a Flavin-Dependent Nadh:Quinone Oxidoreductase. *Protein Sci.* **2019**, *28*, 167−175.

(22) Ha, J. Y.; Min, J. Y.; Lee, S. K.; Kim, H. S.; Kim, D. J.; Kim, K. H.; Lee, H. H.; Kim, H. K.; Yoon, H.-J.; Suh, S. W. Crystal Structure of 2-Nitropropane Dioxygenase Complexed with Fmn and Substrate:

Identification of the Catalytic Base. *J. Biol. Chem.* **2006**, *281*, 18660−18667.
(23) Macheroux, P., Uv-Visible Spectroscopy as a Tool to Study Flavoproteins. In *Flavoprotein Protocols*; Chapman, S. K., Reid, G. A., Eds.; Humana Press: Totowa, NJ, 1999; pp 1−7.
(24) Kabir, M. P.; Orozco-Gonzalez, Y.; Gozem, S. Electronic Spectra of Flavin in Different Redox and Protonation States: A Computational Perspective on the Effect of the Electrostatic Environment. *Phys. Chem. Chem. Phys.* **2019**, *21*, 16526−16537.
(25) Sun, M.; Moore, T. A.; Song, P.-S. Molecular Luminescence Studies of Flavines. *J. Am. Chem. Soc.* **1972**, *94*, 1730−1740.
(26) Yagi, K.; Ohishi, N.; Nishimoto, K.; Choi, J. D.; Song, P.-S. Effect of Hydrogen Bonding on Electronic Spectra and Reactivity of Flavins. *Biochemistry* **1980**, *19*, 1553−1557.
(27) Stanley, R. J.; Jang, H. Electronic Structure Measurements of Oxidized Flavins and Flavin Complexes Using Stark-Effect Spectroscopy. *J. Phys. Chem. A* **1999**, *103*, 8976−8984.
(28) Kodali, G.; Siddiqui, S. U.; Stanley, R. J. Charge Redistribution in Oxidized and Semiquinone E. Coli DNA Photolyase Upon Photoexcitation: Stark Spectroscopy Reveals a Rationale for the Position of Trp382. *J. Am. Chem. Soc.* **2009**, *131*, 4795−4807.
(29) Abramovitz, A. S.; Massey, V. Interaction of Phenols with Old Yellow Enzyme. Physical Evidence for Charge-Transfer Complexes. *J. Biol. Chem.* **1976**, *251*, 5327−5336.
(30) Massey, V.; Ganther, H. On the Interpretation of the Absorption Spectra of Flavoproteins with Special Reference to D-Amino Acid Oxidase. *Biochemistry* **1965**, *4*, 1161−73.
(31) Latovitzki, N.; Halper, J. P.; Beychok, S. Spectrophotometric Titration of Tyrosine Residues in Human Lysozyme. *J. Biol. Chem.* **1971**, *246*, 1457−60.
(32) Schwans, J. P.; Sunden, F.; Gonzalez, A.; Tsai, Y.; Herschlag, D. Uncovering the Determinants of a Highly Perturbed Tyrosine Pka in the Active Site of Ketosteroid Isomerase. *Biochemistry* **2013**, *52*, 7840−7855.
(33) Draper, R. D.; Ingraham, L. L. A Potentiometric Study of the Flavin Semiquinone Equilibrium. *Arch. Biochem. Biophys.* **1968**, *125*, 802−808.
(34) Macheroux, P.; Kappes, B.; Ealick, S. E. Flavogenomics − a Genomic and Structural View of Flavin-Dependent Proteins. *FEBS J.* **2011**, *278*, 2625−2634.
(35) Meyer, T. E.; Bartsch, R. G.; Caffrey, M. S.; Cusanovich, M. A. Redox Potentials of Flavocytochromes C from the Phototrophic Bacteria, Chromatium Vinosum and Chlorobium Thiosulfatophilum. *Arch. Biochem. Biophys.* **1991**, *287*, 128−34.
(36) Stenberg, K.; Clausen, T.; Lindqvist, Y.; Macheroux, P. Involvement of Tyr24 and Trp108 in Substrate Binding and Substrate Specificity of Glycolate Oxidase. *Eur. J. Biochem.* **1995**, *228*, 408−16.
(37) Orozco-Gonzalez, Y.; Kabir, M. P.; Gozem, S. Electrostatic Spectral Tuning Maps for Biological Chromophores. *J. Phys. Chem. B* **2019**, *123*, 4813−4824.
(38) Raffelberg, S.; Gutt, A.; Gartner, W.; Mandalari, C.; Abbruzzetti, S.; Viappiani, C.; Losi, A. The Amino Acids Surrounding the Flavin 7a-Methyl Group Determine the Uva Spectral Features of a Lov Protein. *Biol. Chem.* **2013**, *394*, 1517−28.
(39) Canuto, S. *Solvation Effects on Molecules and Biomolecules: Computational Methods and Applications*; Springer Science & Business Media: 2010; Vol. *6*.
(40) Coutinho, K.; Georg, H. C.; Fonseca, T. L.; Ludwig, V.; Canuto, S. An Efficient Statistically Converged Average Configuration for Solvent Effects. *Chem. Phys. Lett.* **2007**, *437*, 148−152.
(41) Hirao, H.; Nagae, Y.; Nagaoka, M. Transition-State Optimization by the Free Energy Gradient Method: Application to Aqueous-Phase Menshutkin Reaction between Ammonia and Methyl Chloride. *Chem. Phys. Lett.* **2001**, *348*, 350−356.
(42) Okuyama-Yoshida, N.; Kataoka, K.; Nagaoka, M.; Yamabe, T. Structure Optimization Via Free Energy Gradient Method: Application to Glycine Zwitterion in Aqueous Solution. *J. Chem. Phys.* **2000**, *113*, 3519−3524.
(43) Okuyama-Yoshida, N.; Nagaoka, M.; Yamabe, T. Transition-State Optimization on Free Energy Surface: Toward Solution Chemical Reaction Ergodography. *Int. J. Quantum Chem.* **1998**, *70*, 95−103.
(44) Orozco-Gonzalez, Y.; et al. An Average Solvent Electrostatic Configuration Protocol for Qm/Mm Free Energy Optimization: Implementation and Application to Rhodopsin Systems. *J. Chem. Theory Comput.* **2017**, *13*, 6391−6404.
(45) Nikolaev, D. M.; Manathunga, M.; Orozco-Gonzalez, Y.; Shtyrov, A. A.; Guerrero Martinez, Y. O.; Gozem, S.; Ryazantsev, M. N.; Coutinho, K.; Canuto, S.; Olivucci, M. Free Energy Computation for an Isomerizing Chromophore in a Molecular Cavity Via the Average Solvent Electrostatic Configuration Model: Applications in Rhodopsin and Rhodopsin-Mimicking Systems. *J. Chem. Theory Comput.* **2021**, DOI: 10.1021/acs.jctc.1c00221.
(46) Iyer, A.; et al. A Single-Point Mutation in D-Arginine Dehydrogenase Unlocks a Transient Conformational State Resulting in Altered Cofactor Reactivity. *Biochemistry* **2021**, *60*, 711−724.
(47) Cembran, A.; Bernardi, F.; Olivucci, M.; Garavelli, M. The Retinal Chromophore/Chloride Ion Pair: Structure of the Photoisomerization Path and Interplay of Charge Transfer and Covalent States. *Proc. Natl. Acad. Sci. U. S. A.* **2005**, *102*, 6255.
(48) Pedraza-González, L.; De Vico, L.; Marín, M. a. d. C.; Fanelli, F.; Olivucci, M. A-Arm: Automatic Rhodopsin Modeling with Chromophore Cavity Generation, Ionization State Selection, and External Counterion Placement. *J. Chem. Theory Comput.* **2019**, *15*, 3134−3152.
(49) Rinaldi, S.; Melaccio, F.; Gozem, S.; Fanelli, F.; Olivucci, M. Comparison of the Isomerization Mechanisms of Human Melanopsin and Invertebrate and Vertebrate Rhodopsins. *Proc. Natl. Acad. Sci. U. S. A.* **2014**, *111*, 1714.
(50) Tazhigulov, R. N.; Bravaya, K. B. Free Energies of Redox Half-Reactions from First-Principles Calculations. *J. Phys. Chem. Lett.* **2016**, *7*, 2490−2495.
(51) Tazhigulov, R. N.; Gurunathan, P. K.; Kim, Y.; Slipchenko, L. V.; Bravaya, K. B. Polarizable Embedding for Simulating Redox Potentials of Biomolecules. *Phys. Chem. Chem. Phys.* **2019**, *21*, 11642−11650.
(52) Sulpizi, M.; Raugei, S.; VandeVondele, J.; Carloni, P.; Sprik, M. Calculation of Redox Properties: Understanding Short- and Long-Range Effects in Rubredoxin. *J. Phys. Chem. B* **2007**, *111*, 3969−3976.
(53) Warshel, A.; Dryga, A. Simulating Electrostatic Energies in Proteins: Perspectives and Some Recent Studies of Pkas, Redox, and Other Crucial Functional Properties. *Proteins: Struct., Funct., Genet.* **2011**, *79*, 3469−3484.
(54) Hückel, E.; Debye, P. The Theory of Electrolytes: I. Lowering of Freezing Point and Related Phenomena. *Phys. Z.* **1923**, *24*, 1.
(55) Inoue, H.; Nojima, H.; Okayama, H. High Efficiency Transformation of Escherichia Coli with Plasmids. *Gene* **1990**, *96*, 23−28.
(56) Bradford, M. M. A Rapid and Sensitive Method for the Quantitation of Microgram Quantities of Protein Utilizing the Principle of Protein-Dye Binding. *Anal. Biochem.* **1976**, *72*, 248−254.
(57) Whitby, L. G. A New Method for Preparing Flavin-Adenine Dinucleotide. *Biochemical journal* **1953**, *54*, 437−42.
(58) Allison, D.; Purich, D. L., Practical Considerations in the Design of Initial Velocity Enzyme Rate Assays. In *Contemporary Enzyme Kinetics and Mechanism*, 3rd. ed.; Purich, D. L., Ed.; Academic Press: Cambridge, MA, 1979.
(59) Ferré, N.; Ángyán, J. G. Approximate Electrostatic Interaction Operator for Qm/Mm Calculations. *Chem. Phys. Lett.* **2002**, *356*, 331−339.
(60) Singh, U. C.; Kollman, P. A. A Combined Ab Initio Quantum Mechanical and Molecular Mechanical Method for Carrying out Simulations on Complex Molecular Systems: Applications to the Ch3cl+ Cl− Exchange Reaction and Gas Phase Protonation of Polyethers. *J. Comput. Chem.* **1986**, *7*, 718−730.
(61) Humbel, S.; Sieber, S.; Morokuma, K. The Imomo Method: Integration of Different Levels of Molecular Orbital Approximations

for Geometry Optimization of Large Systems: Test for N-Butane Conformation and Sn 2 Reaction: Rcl+ Cl−. *J. Chem. Phys.* **1996**, *105*, 1959−1967.
(62) Abraham, M. J.; Murtola, T.; Schulz, R.; Páll, S.; Smith, J. C.; Hess, B.; Lindahl, E. Gromacs: High Performance Molecular Simulations through Multi-Level Parallelism from Laptops to Supercomputers. *SoftwareX* **2015**, *1*, 19−25.
(63) Hornak, V.; Abel, R.; Okur, A.; Strockbine, B.; Roitberg, A.; Simmerling, C. Comparison of Multiple Amber Force Fields and Development of Improved Protein Backbone Parameters. *Proteins: Struct., Funct., Genet.* **2006**, *65*, 712−25.
(64) Jorgensen, W. L.; Chandrasekhar, J.; Madura, J. D.; Impey, R. W.; Klein, M. L. Comparison of Simple Potential Functions for Simulating Liquid Water. *J. Chem. Phys.* **1983**, *79*, 926−935.
(65) Darden, T.; York, D.; Pedersen, L. Particle Mesh Ewald - an N.Log(N) Method for Ewald Sums in Large Systems. *J. Chem. Phys.* **1993**, *98*, 10089−10092.
(66) Malde, A. K.; Zuo, L.; Breeze, M.; Stroet, M.; Poger, D.; Nair, P. C.; Oostenbrink, C.; Mark, A. E. An Automated Force Field Topology Builder (Atb) and Repository: Version 1.0. *J. Chem. Theory Comput.* **2011**, *7*, 4026−4037.
(67) Roos, B. O.; Taylor, P. R.; Sigbahn, P. E. M. A Complete Active Space Scf Method (Casscf) Using a Density Matrix Formulated Super-Ci Approach. *Chem. Phys.* **1980**, *48*, 157−173.
(68) Widmark, P.-O.; Malmqvist, P.-Å.; Roos, B. O. Density Matrix Averaged Atomic Natural Orbital (Ano) Basis Sets for Correlated Molecular Wave Functions. *Theoretica chimica acta* **1990**, *77*, 291−306.
(69) Andersson, K.; Malmqvist, P. A.; Roos, B. O.; Sadlej, A. J.; Wolinski, K. Second-Order Perturbation Theory with a Casscf Reference Function. *J. Phys. Chem.* **1990**, *94*, 5483−5488.
(70) Sørensen, L. K.; Guo, M.; Lindh, R.; Lundberg, M. Applications to Metal K Pre-Edges of Transition Metal Dimers Illustrate the Approximate Origin Independence for the Intensities in the Length Representation. *Mol. Phys.* **2017**, *115*, 174−189.
(71) Choe, Y.-K.; Nagase, S.; Nishimoto, K. Theoretical Study of the Electronic Spectra of Oxidized and Reduced States of Lumiflavin and Its Derivative. *J. Comput. Chem.* **2007**, *28*, 727−739.
(72) Karasulu, B.; Götze, J. P.; Thiel, W. Assessment of Franck−Condon Methods for Computing Vibrationally Broadened Uv−Vis Absorption Spectra of Flavin Derivatives: Riboflavin, Roseoflavin, and 5-Thioflavin. *J. Chem. Theory Comput.* **2014**, *10*, 5549−5566.
(73) Klaumünzer, B.; Kröner, D.; Saalfrank, P. (Td-)Dft Calculation of Vibrational and Vibronic Spectra of Riboflavin in Solution. *J. Phys. Chem. B* **2010**, *114*, 10826−10834.
(74) Kabir, M. P.; Orozco-Gonzalez, Y.; Hastings, G.; Gozem, S. The Effect of Hydrogen-Bonding on Flavin's Infrared Absorption Spectrum. *Spectrochim. Acta, Part A* **2021**, *262*, 120110.
(75) Su, D.; Kabir, M. P.; Orozco-Gonzalez, Y.; Gozem, S.; Gadda, G. Fluorescence Properties of Flavin Semiquinone Radicals in Nitronate Monooxygenase. *ChemBioChem* **2019**, *20*, 1646−1652.
(76) Ponder, J. W.; Case, D. A. Force Fields for Protein Simulations. *Adv. Protein Chem.* **2003**, *66*, 27−85.
(77) Fdez. Galvan, I.; et al. Openmolcas: From Source Code to Insight. *J. Chem. Theory Comput.* **2019**, *15*, 5925−5964.
(78) Frisch, M. J.; et al. *Gaussian 16* Rev. C.01; Gaussian: Wallingford, CT, 2016.

https://doi.org/10.1021/acs.jpclett.1c02173
J. Phys. Chem. Lett. 2021, 12, 8384−8396